Reduced Coulomb interaction in organic solar cells by the introduction of high-*k* $SrTiO_3$ nanoparticles

Niels Benson[1], Miriam Engel[1], David Schaefer[2], Daniel Erni[2], Julia Kern[3], Carsten Deibel[3], Eva M. Herzig[4], Peter Müller – Buschbaum[5] and Roland Schmechel[1]

[1] NST / University of Duisburg – Essen and CENIDE, Duisburg, NRW, 47057, Germany
[2] ATE / University of Duisburg – Essen and CENIDE, Duisburg, NRW, 47057, Germany
[3] Experimental Physics VI / Julius-Maximilian University of Würzburg, 97074 Würzburg, Germany
[4] Munich School of Engineering / Technische Universität München, 85747 Garching, Germany,
[5] Lehrstuhl für Funktionelle Materialien / Technische Universität München, 85747 Garching, Germany

***ABSTRACT* — A concept is introduced which allows for reduced Coulomb interaction in organic solar cells and as such for enhanced power conversion efficiencies. The concept is based on the introduction of electrically insulating, nanostructured high-*k* materials into the organic matrix, which do not contribute to the charge carrier transport, however, enhance the effective permittivity of the organic active layer.Using an analytical model, it is demonstrated that even at a distance of 20 nm to the organic / inorganic interface of the nanostructure, the Coulomb interaction in the organic semiconductor can be reduced by more than 15 %. The concept is substantiated experimentally by realizing P3HT:PCBM solar cells with integrated $SrTiO_3$ nanoparticles. It could be demonstrated that in comparison to a reference cells without nanoparticles, the power conversion efficiency is improved by ~17 %. This effect is interpreted to be the result of an organic active layer effective permittivity enhancement, which is supported by the result of transient absorption as well as grazing incidence wide angle x – ray scattering measurements.**

***Index Terms* — Organic PV, high-k organic semiconductors, reduced Coulomb interaction**

I. Introduction

During the last decade an increase in the power conversion efficiency of organic photovoltaic cells up to almost 11 % could be realized [1]. This is mainly the result of developments in the device and material design, as well as optimized morphologies. Widely used is the bulk-heterojunction concept [2] as well as tandem solar cell designs [3]. However, one aspect which has received little attention during this development is the high Coulomb interaction in organic semiconductors, as a result of the low semiconductor permittivity (ε_r ~ 3-4). This material property contributes to high exciton binding energies of up to 1.4 eV [4], reduces charge transport properties due to electrostatic interaction and leads to enhanced geminate pair formation [2, 5]. An enhancement of the material permittivity would reduce the influence of the Coulomb interaction and therefore have a beneficial effect on the maximum obtainable power conversion efficiency for organic solar cells. This can be achieved either by designing novel organic semiconductor materials with an enhanced permittivity [6], or by enhancing the effective permittivity of the organic active layer. The later has been recently demonstrated by facilitated exciton separation in pentacene on high-*k* substrates [7]. In the following, a summary of one of our current publications [8] is discussed using an analytical simulation as well as a P3HT:PCBM material system with and without integrated $SrTiO_s$ nanoparticles, to demonstrate the feasibility of a concept which allows to enhance the effective permittivity of organic solar cells by the integration of electrically insulating, nanostructured high-*k* materials. This discussion is extended by transient absorption spectroscopy (TAS) as well as grazing incidence wide angle x – ray scattering (GIWAXS) measurements and interpretation.

II. Experimental

Samples were prepared on commercially available OLED grade glass substrates covered with indium tin oxide (OPV devices, TAS) as well as crystalline Si substrates with a native SiOx layer. Poly(3,4-ethylenedioxythiophene) poly(styrene-sulfonate) (PEDOT:PSS, Clevios P VPAl 4083) was spin coated on all substrates and subsequently annealed for 10 min at 165 °C. All further processing was conducted in inert N_2 atmosphere. The active layer for both high-*k* and reference devices was prepared using a 1:0.78 blend of regioregular poly(3-hexylthiophene-2,5-diyl) (P3HT, Sepiolid P200, BASF) and [6,6]-phenyl-C61-butyric acid methyl ester (PCBM, Sigma Aldrich) solved in chlorobenzene (10 mg ml^{-1} P3HT). To realize high-*k* P3HT:PCBM thin films, dried (150 °C under vacuum, 2 h) strontium titanate ($SrTiO_3$, Iolitec) nanoparticles were added to a part of the reference solution, already stirred at 65-70 °C for 8 h in a concentration of 5 mg ml^{-1}. Further, Ceramic grinding balls were added to the high-*k* solution for better nanoparitcle dispersability. Both low-*k* solution and high-*k* dispersion were continuously stirred

over night. Prior to the spin coating procedure for organic thin film deposition, the low-*k* solution and high-*k* dispersion were filtered using a combination of 2.7 µm, 1.2 µm and 0.7 filters. For the purpose of photovoltaic devices manufacturing (20 mm² active area), Metal electrodes (50 nm Ca, 150 nm Al) were deposited by physical vapor deposition at a chamber base pressure of 10^{-6}mbar. In a final step all devices were annealed for 10 min at 140 °C.

Electrical characterization was done using a Keithley source-measure unit in the dark and under standard AM1.5 illumination in N_2 atmosphere.

TAS experiments were conducted in high vacuum. For the measurement samples were optically pumped by a frequency doubled Nd:YaG laser (532nm) using 7 ns pulses with a laser fluence of 26.5µJ / cm^2, and probed using CW 977nm radiation gained from a 100W Xenon lamp in combination with an AMKO LTI monochromator. The absorption decay was recorded using an InGaAs photodiode in combination with a Femto HCA-S-400M-In preamplifier connected to a Tektronix TDS 3034 Oscilloscope.

GIWAXS measurements were conducted at the BW4, Doris III, Desy in ambient atmosphere, using a wavelength of 0.138nm at an incidence angle of 0.18°. The scattering was detected using a MarCCD 165 area detector at a sample detector distance of 105mm

III. Theory

In order to quantify the influence of the organic / high-*k* material interface on the electrostatic charge carrier interaction in organic semiconductors, the following analytical model is used to describe the Coulomb interaction between complementary charges at the interface between low-*k* and high-*k* infinite large half-spaces. The model considers a stationary charge Q_s in a low-*k* material at a distance of 2.5 nm to a low-*k* / high-*k* interface, as well as a reference low-*k* / low-*k* interface. The model investigates the interaction of a test charge with the stationary charge. Further, image charges induced at the interface by the stationary and the test charges are considered. Both test and stationary charges carry a charge equal to $|Q| = nq$. Whereby n is 1 and q is the elementary charge.

The electrostatic interaction between the respective charges is described by the Coulomb interaction, with a force $F_{Coulomb}$. The bound charge density induced by the charges Q_s or Q_t, is each described as a single image charge Q' using the following equation [9]:

$$Q' = \frac{\varepsilon_{r,low-k} - \varepsilon_{r,high-k}}{\varepsilon_{r,low-k} + \varepsilon_{r,high-k}} Q \qquad (1)$$

Equation 1 is valid for test charge interaction in the low-*k* half space. The interaction scenarios considered here are Case A (the reference system) with a low-*k* / low-*k* interface. Both half spaces are assigned a permittivity of 3. For case B a low-*k* / high-*k* interface is taken into account. Here respective permittivities of 3 and 300 are considered for the low-*k* / high-*k* material. In consequence only the Coulomb interaction between the stationary charge Q_s and the test charge Q_t needs to be considered for case A, while for case B an additional interaction with the image charges Q_s' and Q_t' needs to be considered.

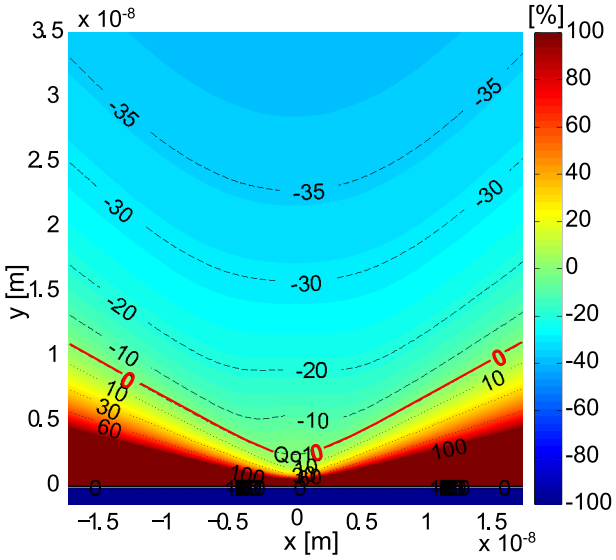

Fig. 1. Change in the escape energy between cases A and B.

To analyze the total Coulomb force influencing the test charge, the concept of the escape energy E_{escape} is introduced. It describes the total energy input needed to move Q_t into infinity, and can therefore be related to the difference in potential energy ΔE_{pot} of the test charge at position P_a and the reference point P_∞ at infinity. The escape energy E_{escape} is calculated by integrating the effort to counteract the total Coulomb force $\vec{F}$ affecting the test charge as shown in Eq. 2.

$$E_{escape} = -\Delta E_{pot} = -\int_{P_a}^{P_\infty} \vec{F} \cdot d\vec{s} = -Q_t \cdot \varphi_{total}(P_a) \qquad (2)$$

Here $\vec{E}$ describes the electric field. The electrical potential at P_∞ is considered to be zero. It is evident that the escape energy E_{escape} of the test charge can be calculated by the multiplication of the test charge Q_t with the total electrical potential φ_{total} at position P_a. The potential φ_{total} is analytically calculated by a superposition of the potential of the stationary charge Q_s as well as the image charges Q_s' and Q_t' ($\varphi_{total} = \varphi_s + \varphi_{s'} + \varphi_{t'}$).

Please note that the presented formalism for the total potential φ_{total} bears a minor subtlety due to a simultaneous movement of the image charge Q_t' during the "escape" of the test charge Q_t. Even though a direct contribution from Q_t will alter the total potential φ_{total} according to its changing position, and therefore a changing position of Q_t', it is not relevant whether the image charge Q_t' is doing work or not. Here, we are focusing on the escape process only, leaving aside the

changing energy input (due to polarization) into the high-*k* material.

The result of this escape energy evaluation is illustrated in Fig. 1, as the change in escape energy between the cases A and B. The graph demonstrates that the benefit of a reduced escape energy due to the introduction of a high-*k* interface increases, with an increase in the test charge / interface distance. At a distance of 20 nm to the stationary charge and perpendicular to the high-*k* interface, a reduction of the escape energy by 30 % is found. At a distance of 45 nm the escape energy is even reduced by over 40 %.

For case B the reduced interaction between the stationary charge and the test charge can be ascribed to a screening of the stationary charge Q_s by its image charge Q_s'. Here, the screening results into an effective Q_s of:

$$Q_{s,effective} = \left(1 + \frac{\varepsilon_{r,low\text{-}k} - \varepsilon_{r,high\text{-}k}}{\varepsilon_{r,low\text{-}k} + \varepsilon_{r,high\text{-}k}}\right) \cdot Q_s \approx 0.02 \cdot Q_s \quad (3)$$

While this effect may be beneficial for test charges at a distance to the high-*k* interface beyond the red dashed 0 % relative escape energy change line as indicated in Fig. 1, an enhancement in the escape energy is found for test charges close to the high-*k* interface due to image charge interaction. However, in this region the Coulomb force has a major component perpendicular to the interface. In consequence, charge carrier transport in parallel to the high-*k* interface does not require additional energy. Therefore, if charge carrier transport parallel to the high-k interface is possible in organic pv device structures, for example by the integration of electrcally insulating high-k percolatoin paths between the anode-cathode, the interface interaction will not limit electronic transport in such devices and therefore not limit the benefit of the effectivly enhanced organic semiconductor permittivity for organic pv applications.

IV. First Devices

To test the feasibility of the discussed concept for an organic pv application, first P3HT:PCBM devices containing evenly distributed high-*k* $SrTiO_3$ percolating nanoparticle agglomerates were implemented. The anode-cathode percolation path ensures a) charge carrier transport through the device parallel to the high-*k* interface as discussed above, and b) unproblematic charge carrier extraction at the electrodes, as the permittivity of the electrodes exceeds the permittivity of the $SrTiO_3$.

Illustrated in Fig. 2 is the current voltage characteristic of a P3HT:PCBM:$SrTiO_3$ device in comparison to a P3HT:PCBM reference. The devices were measured in the dark as well as under AM1.5 standard illumination. In comparison to the reference device, the short circuit current for the high-*k* cell has been reduced by ~3.6 % from J_{sc} = 7.9 mA cm^{-2} down to J_{sc} ~ 7. mA cm^{-2}. The fill factors (*FF*) on the other hand, as well as the open circuit voltages (V_{oc}) have been improved by ~ 10 %. The *FF* shows an improvement from 0.49 (reference) up to 0.54 (high-*k*), while the open circuit voltage has been increased from V_{oc} = 0.52 V (reference) up to V_{oc} = 0.57 V (high-*k*). In terms of power conversion efficiency, this translates into an efficiency improvement for the high-*k* solar cell of ~17 % from η = 2 % absolute for the reference cell up to η = 2.34 % absolute for the high-*k* cell. Statistical data confirming the discussed performance enhancement for high-*k* organic devices is illustrated in Tab. I. Here, average values of two P3HT:PCBM reference devices are compared with the average values of seven SrTiO3:P3HT:PCBM devices. Further, the two sigma standard deviation is specified for the SrTiO3:P3HT:PCBM cells. A relatively high standard deviation is found for the η and J_{sc} values, which are each the consequence of a higher deviation for one out of the seven high-*k* cells. These outlier cells are suggested to be the result of non optimized process conditions. The obtained low absolute efficiencies of ~ 2 % for both reference and high-*k* devices are ascribed to the extensive stirring times of ~ 24 h at *T* = 65-70 °C in order to disperse the SrTiO3 nanoparticles in the P3HT:PCBM solution, and therefore to semiconductor degradation effects.

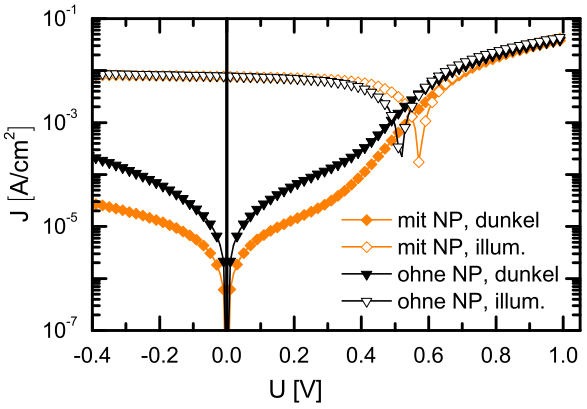

Fig. 2. *I*(*V*)-characteristics of a P3HT:PCBM:$SrTiO_3$ solar cell and of a P3HT:PCBM reference device.

Transmission and reflection properties remain the same upon nanoparticle integration into the P3HT:PCBM matrix, as discussed elsewhere [8]. In consequence we conclude that the obtained power conversion efficiency improvement for the

TABLE I
AVERAGE SOLAR CELL PARAMETERS AND 2σ STANDARD DEVIATION

	η_{ave} [%]	2σ	$V_{oc,\,avg}$ [V]	2σ	$J_{sc,\,avg}$ [mA cm^{-2}]	2σ	FF	2σ
P3HT:PCBM (2 cells)	2.07	-	0.54	-	8.11	-	0.48	-
SrTiO3:P3HT:PCBM (7 cells)	2.25	0.46	0.57	0.016	7.73	0.86	0.51	0.0654

organic solar cell with integrated nanoparticles is not the result of light-scattering effects and as such an enhanced optical path length within the cell. Instead we suggest the enhanced power conversion efficiency of the solar cells with integrated $SrTiO_3$ particles to be the result of an effectively enhanced device permittivty. The development of J_{sc} and V_{oc} upon nanoparticle integration supports this statement. For P3HT:PCBM organic solar cells, with an exciton separation efficiency close to 100%, at the acceptor / donor heterointerface, no significant further improvement of the exciton separation efficiency is expected, and therefore no improvement in the short circuit current [10]. However, due to the enhancement of the effective system permittivity, we anticipate a reduction of the non-geminate recombination probability during charge carrier transport as the result of reduced Coulomb interaction and therefore the observed increase in V_{oc} [8].

To further support this interpretation, TAS measurements were conducted to investigate the influence of the high-*k* nanoparticle integration and therefore the effective permittivity enhancement on the charge carrier lifetime. The result of the measurement is illustrated in Fig. 3, comparing the TAS transient of P3HT:PCBM and P3HT:PCBM:$SrTiO_3$ thin films. For better comparability both transients are normalized to unity at t = 10ns.

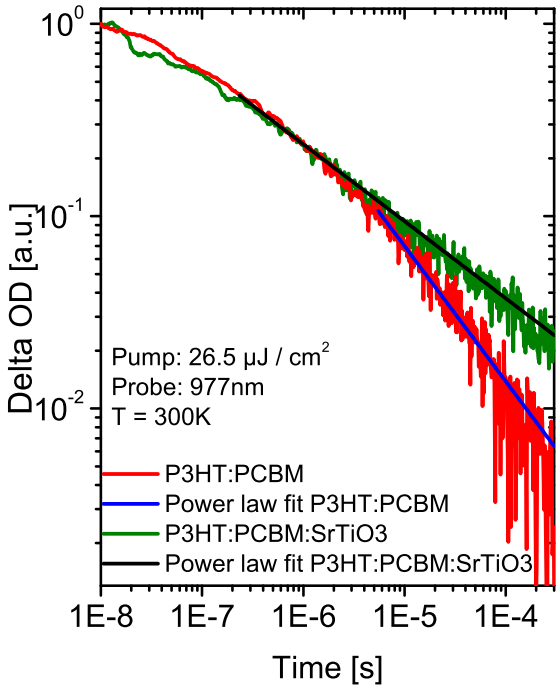

Fig. 3. Comparison of TAS transients for P3HT:PCBM thin films with and without $SrTiO_3$ nanoparticles. Both transients are normalized to unity at t = 10ns. The gradient of respective power law fits is an indication for the rate of bimolecular recombination.

The rate of bimolecular recombination is determined by fitting the transients using a power law dependence ($\Delta OD \sim t^{-\alpha}$) [11]. This fit is conducted for measurement times > 100ns, in order to be able to neglect the influence of the recording setup response time on the transient signal [12]. Due to the $SrTiO_3$ nanoparticle integration into the P3HT:PCBM thin film, the gradient of the power law decay has been reduced from $\alpha \sim$ -0.7 down to $\alpha \sim$ -0.4. This indicates a longer charge carrier lifetime and therefore a reduction in bimolecular recombination [11]. Considering the used organic semiconductor blend and the laser fluence used to pump the system, it is assumed that only trap limited recombination is found in the recorded transients [11, 13]. Without additional information, it is therefore not possible to conclude whether this enhanced charge carrier lifetime is the result of nanoparticle induced morphological disorder, or a result of the effectively enhanced permittivity. As outlined above, the interaction of charge carriers with induced image charges will lead to charge carrier attraction to the high-*k* interface. While this effect is no limitation to the introduced solar cell concept, as long as charge carrier transport parallel to the high-*k* interface is possible, the transient absorption measurement will be influenced by this effect in the trap limited part of the transient. As no current is flowing during this experiment, the high-k interface will function as a Coulomb trap, leading to the observed extension in charge carrier lifetime.

In order to obtain information about possible thin film morphology changes upon nanoparticle integration, GIWAXS measurements were conducted on P3HT:PCBM thin films with and without integrated $SrTiO_3$ nanoparticles. Fig. 4 a) and b) show the result of the scattering intensity in the vertical and the horizontal direction respectively. The only significant difference between the intensity curves with and without $SrTiO_3$ nanoparticles are the contributions from the $SrTiO_3$. Minor deviations in intensity are ascribed to possible variations in thin film thickness and roughness. The P3HT peak positions and peak widths of the P3HT signal show no changes upon the addition of nanoparticles. Therefore the backbone to backbone separation distance (d) remains almost identical. Only in the (200) orientation a slight increase in the backbone separation distance from 0.82nm to 0.83 nm is detected for the P3HT:PCBM thin film with integrated $SrTiO_3$ nanoparticles. An additional small change due to the nanoparticle integration is found in the polymer π – π stacking determined from the (010) peak position. Here we find that the stacking distance is slightly reduced from 0.38nm down to 0.37nm in the P3HT:PCBM: $SrTiO_3$ thin film. The respective peak positions in the q – space as well as backbone and π – stacking distances for P3HT are summarized in Tab. II.

Considering the result of the GIWAXS measurement, which has only shown a marginal change in the P3HT:PCBM molecular arrangement upon $SrTiO_3$ nanoparticle integration, we suggest the result of the TAS measurement, which is a longer charge carrier lifetime in P3HT:PCBM:$SrTiO_3$ thin films in comparison to the P3HT:PCBM reference, to be the result of an effectively enhanced thin film permittivity. In consequence we propose the obtained power conversion

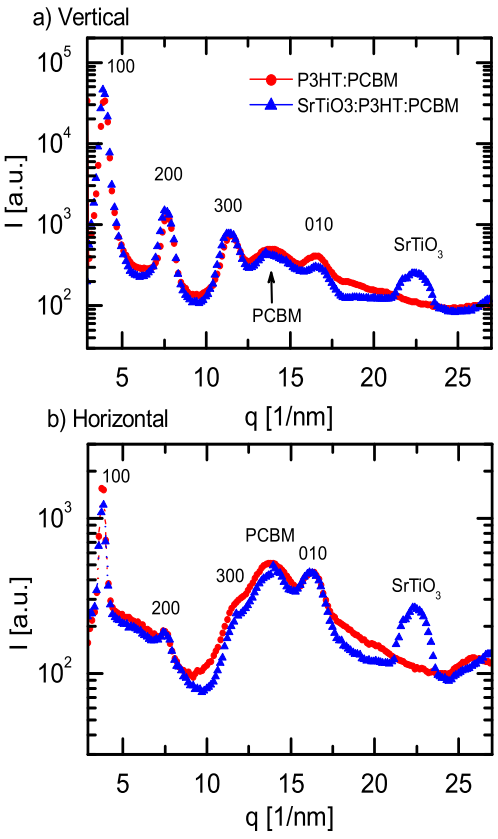

Fig. 4. Scattering intensity curves from the GIWAXS pattern a) for the vertical and b) the in plane direction.

efficiency enhancement of ~ 17% for P3HT:PCBM:$SrTiO_3$ solar cells to be the result of reduced Coulomb interaction and not the consequence of morphology changes.

V. Summary

A new concept to enhance the effective permittivity of organic solar cells, by the integration of electrically insulating, nanostructured high-*k* materials has been introduced. Using an analytical model we substantiated that an enhancement of the effective organic thin film permittivity will reduce the Coulomb interaction in the organic layer, and as such will improve charge carrier transport properties. This was experimentally verified by realizing first P3HT:PCBM:$SrTiO_3$ organic photovoltaic devices, which demonstrate an enhanced power conversion efficiency of ~ 17 % in comparison to a P3HT:PCBM reference device. Using TAS in combination with GIWAXS measurements, we have further shown an enhanced charge carrier lifetime in P3HT:PCBM thin films with integrated $SrTiO_3$ nanoparticles, while only a marginal change in the thin film morphology due to nanoparticle integration has been detected. We therefore suggest the obtained charge carrier lifetime enhancement, as well as the demonstrated power conversion efficiency improvement upon high-*k* nanoparticle integration into the P3HT:PCBM matrix, to be the result of an effectively enhanced permittivity and in consequence a reduced Coulomb interaction.

TABLE II
GIWAXS P3HT, PCBM Peak Positions

	P3HT								PCBM	
	(100)		(200)		(300)		(010)			
1 / nm nm	q	d	q	d	q	d	q	d	q	d
P3HT: PCBM	3.9	1.61	7.7	0.82	11.5	0.55	16.7	0.38	14	0.45
SrTiO3: P3HT: PCBM	3.9	1.61	7.6	0.83	11.4	0.55	16.8	0.37	13.9	0.45

ACKNOWLEDGEMENT

This project is supported by a North Rhine-Westphalia research scholarship for ”rollable solar cells”. Further, the authors gratefully acknowledge the beamline support for the GIWAXS measurements by Jan Perlich, DESY, Notkestr. 85, 22607 Hamburg.

References

[1] M. A. Green, K. Emery, Y. Hishikawa, W. Warta, E. D. Dunlop, ”Solar cell efficiency tables”, *Prog. Photovolt.: Res. Appl.*, vol. 20, pp. 12, 2012.

[2] C. Deibel, V. Dyakonov, ”Polymer–fullerene bulk heterojunction solar cells”, *Rep. Prog. Phys.*, vol. 73, pp. 096401, 2010.

[3] J. Meiss, T. Menke, K. Leo, C. Uhrich, W.-M. Gnehr, S. Sonntag, M. Pfeiffer, M. Riede, ”Highly efficient semi-transparent tandem organic solar cells with complementary absorber materials”, *Appl. Phys. Lett.*, vol. 99, pp. 043301, 2011.

[4] M. Knupfer, "Exciton binding energies in organic semiconductors”, *Appl. Phys. A*, vol. 77, pp. 623, 2003.

[5] L. J. A. Koster, S. E. Shaheen, J. C. Hummelen, ”Pathways to a New Efficiency Regime for Organic Solar Cells”, *Adv. Energy Mater.*, vol. 2, pp. 1246 2012.

[6] M. Lenes, F. B. Kooistra, J. C. Hummelen, I. Van Severen, L. Lutsen, D. Vanderzande, T. J. Cleij, P. W. M. Blom, J., ”Chare dissociation in polymer:fullerene bulk heterojunction solar cells with enhanced permittivity”,*Appl. Phys.,* vol. 104, pp. 114517, 2008.

[7] M. Engel, F. Kunze, D.C. Lupascu, N. Benson, R. Schmechel, ”Reduced exciton binding energy in organic semiconductors: Tailoring the Coulomb interation”, *Phys. Status Solidi RRL*, vol. *6*, pp. 68, 2012.

[8] M. Engel, D. Schaefer, D. Erni, N. Benson, R. Schmechel, ”Reduced Coulomb interaction in organic solar cells by the introduction of inorganic high-*k* nanostructured materials”, *Phys. Status Solidi A*, vol. *1-7*, DOI 10.1002/ pssa.201228771, 2013.

[9] J. D. Jackson, *Classical Electrodynamics*, New York, John Wiley & Sons, , 1998.

[10] J. Guo, H. Ohkita, H. Benten, S. Ito, ”Charge Generation and Recombination Dynamics in Poly(3-hexylthiophene)/Fullerene

Blend Films with Different Regioregularities and Morphologies", *J. Am. Chem. Soc*., vol. 132, pp. 6154, 2010.

[11] T. M. Clarke, F. C. Jamieson, J. R. Durrant, "Transient Absorption Studies of Bimolecular Recombination Dynamics in Polythiophene / Fullerene Blend Films", *J. Phys- Chem. C*, vol. 113, pp. 20934, 2009.

[12] T. J. Savenije, D. H. K. Murthy, M. Gunz, J. Gorenflot, L. D. A. Siebbeles, V. Dyakonov, C. Deibel, "Absence of Postnanosecond Charge Carrier Relaxation in Poly(3-hxylthiophene)/Fullerene Blends", *J. Phys. Chem. Lett*., vol. 2, pp. 1368, 2011.

[13] M. P. Eng., P. R. F. Barnes, J. R. Durrant, "Concentration-Dependent Hole Mobility and Recombination Coefficient in Bulk Heterojunctions Determined from Transient Absorption Spectroscopy", *J. Phys. Chem. Lett.*, vol. 1, pp. 3096, 2010.